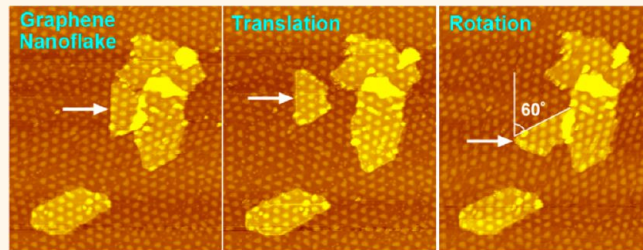


Superlubric Sliding of Graphene Nanoflakes on Graphene

Xiaofeng Feng,^{†,‡} Sangku Kwon,[§] Jeong Young Park,[§] and Miquel Salmeron^{†,‡,*}

[†]Materials Sciences Division, Lawrence Berkeley National Laboratory, Berkeley, California 94720, United States, [‡]Department of Materials Science and Engineering, University of California, Berkeley, California 94720, United States, and [§]Graduate School of E�WS (WCU), KAIST, Daejeon 305-701, Republic of Korea

ABSTRACT The lubricating properties of graphite and graphene have been intensely studied by sliding a frictional force microscope tip against them to understand the origin of the observed low friction. In contrast, the relative motion of free graphene layers remains poorly understood. Here we report a study of the sliding behavior of graphene nanoflakes (GNFs) on a graphene surface. Using scanning tunneling microscopy, we found that the GNFs show facile translational and rotational motions between commensurate initial and final states at temperatures as low as 5 K. The motion is initiated by a tip-induced transition of the flakes from a commensurate to an incommensurate registry with the underlying graphene layer (the superlubric state), followed by rapid sliding until another commensurate position is reached. Counterintuitively, the average sliding distance of the flakes is larger at 5 K than at 77 K, indicating that thermal fluctuations are likely to trigger their transitions from superlubric back to commensurate ground states.



KEYWORDS: graphene nanoflakes · sliding · superlubricity · incommensurability · scanning tunneling microscopy

Understanding the relative motions of two contacting surfaces is essential for controlling friction and lubrication in mechanical systems.¹ An important technique for nanotribological study is frictional force microscopy (FFM), which makes it possible to measure the lateral frictional force between a sharp tip and a surface.^{1,2} One of the most intriguing materials for tribology is graphite, which has been widely used as a solid lubricant in mechanical devices. Its lamellar structure and weak bonding between atomic layers facilitate shear between adjacent layers, which is at the origin of the low-friction characteristics. The sliding between neighboring graphene layers is of great interest, not only toward a deeper understanding of nanotribological phenomena but also for potential applications of graphene flakes in nanolubrication, nanomotors, and moveable components in nanoelectromechanical systems (NEMS).^{3–5}

Most experimental studies of the frictional properties of graphite are carried out using a slider (the tip of the FFM),^{6,7} sometimes with a graphene flake purposely attached to it,⁸ against a graphite or graphene surface. For example, Dienwiebel *et al.* studied the

friction between an FFM tip with an attached flake and a graphite substrate and observed the phenomenon of extremely low friction or “superlubricity”,^{8–10} when the two contacting graphite layers were oriented relative to each other to form an incommensurate interface. The concept of superlubricity was first proposed and investigated by Shinjo and Hirano.^{11,12} Ultralow friction has also been observed between the neighboring layers in multiwall carbon nanotubes.¹³ Along the same lines, it has been reported that micro-meter size graphite flakes can retract back to their initial positions after displacements from their equilibrium configuration.^{14,15}

Recently, several theoretical studies have discussed the sliding of free graphene layers on graphite or graphene substrates, *i.e.*, without being attached to a slider.^{16–19} To date however, very few experimental results have been reported about the dynamics of free graphene flakes and their motions when displaced out of their equilibrium configuration. Such studies, which could provide new data for a more direct comparison with theory, can be performed using noncontact probes such as scanning tunneling microscopy (STM) and noncontact atomic force

* Address correspondence to mbsalmeron@lbl.gov.

Received for review December 11, 2012 and accepted January 17, 2013.

Published online January 17, 2013
10.1021/nn305722d

© 2013 American Chemical Society

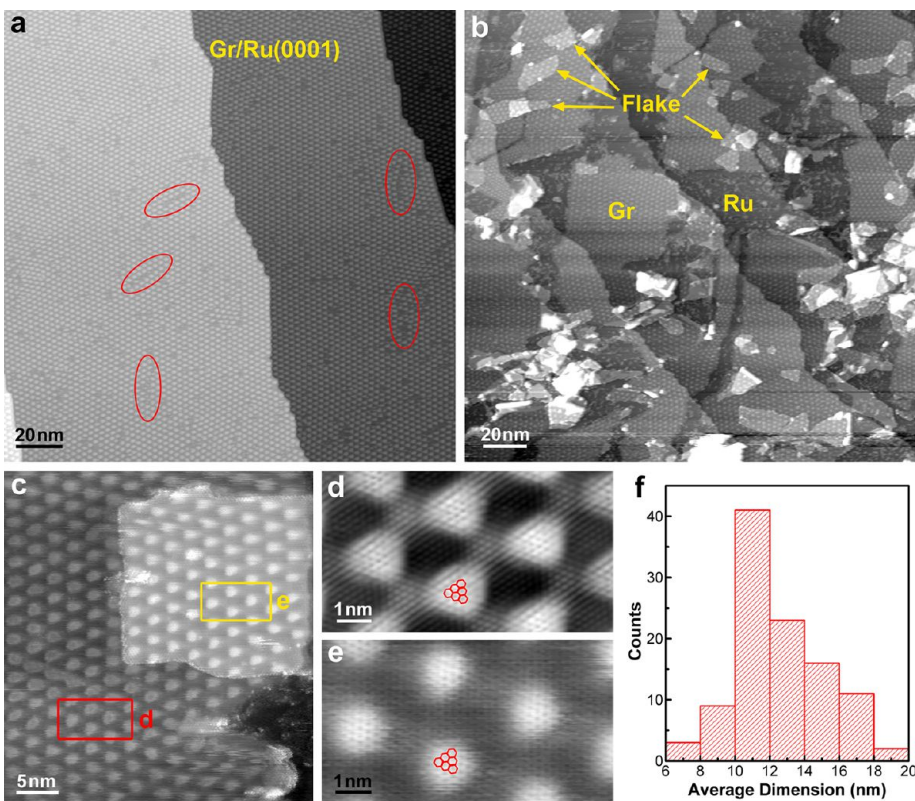


Figure 1. Graphene nanoflakes (GNFs) formed by water-induced splitting of an epitaxial graphene layer on Ru(0001). (a) STM image of the as-grown graphene film on the Ru surface before water adsorption. A few line defects are indicated by red circles. (b) Water adsorption at 110 K caused the graphene film to split into numerous flakes, and some of them were displaced on top of the first graphene layer, as indicated by the arrows. (c–e) Expanded STM images of the first graphene layer with a flake on it, both showing similar Moiré patterns. The atomic lattice structures of the two graphene layers are shown in (d) and (e), indicating that they are commensurately stacked. (f) Statistical size distribution of the flakes. Imaging parameters: (a) $V_s = 150$ mV, $I_t = 15$ pA; (b) $V_s = -2.5$ V, $I_t = 5$ pA; (c–e) $V_s = -15$ mV, $I_t = 500$ pA.

microscopy (NC-AFM). STM studies are the subject of the work presented here.

RESULTS AND DISCUSSION

Recently, we found that water can split an epitaxial graphene layer on Ru(0001) along line defects, resulting in the formation of nanoscale flakes.²⁰ Figure 1a shows an STM image of the graphene layer grown on a Ru(0001) surface. It exhibits a Moiré pattern with a periodicity of about 3 nm that arises from the lattice mismatch between the graphene and Ru substrate.²¹ The expanded STM image in Figure 1d reveals its atomic structure, which corresponds to a C(12×12)–Ru(11×11)²¹ or C(25×25)–Ru(23×23)²² superstructure. Some areas of the graphene are almost defect-free, while defects such as dislocations²³ and grain boundaries²⁴ are found in several areas of the film, as shown in Figure 1a and Figure S1 in the Supporting Information, where broken and stretched bonds are expected to occur. After the adsorption of submonolayer amounts of water at 110 K, the defective graphene area was found to be split into fragments along those line defects,²⁰ as shown in Figure 1b. Some flakes were detached from the Ru substrate due to water intercalation and displaced to other areas, forming

graphene nanoflakes (GNFs) sitting on top of the first graphene layer (see more examples in Figure S2 in the Supporting Information). The splitting of graphene is facilitated by the strong bonding between graphene and Ru, which expands and weakens the C–C bonds,²² thus enhancing their chemical reactivity.^{25,26} The increased strain at the defects can further enhance their reactivity and make them more fragile than the bulk.²⁷

Figure 1c shows an STM image of a flake on top of the first graphene layer, with an expanded view of their lattice structures in Figure 1d and e, respectively. As can be seen, the flake shows the same lattice orientation as that of the underlying graphene layer, indicative of commensurate stacking, which is the most stable configuration.²⁸ The flake shows the same Moiré pattern as the first layer, because it follows the corrugation of the underlying graphene.²⁹ The STM apparent height of the second-layer graphene is around 1.8 ± 0.1 Å at negative sample bias voltages,³⁰ which is smaller than the interlayer distance (~ 3.2 Å),³¹ as the second layer is less doped than the first one and has smaller density of states near the Fermi level,³² resulting in the observed apparent height.³³ The size distribution of the flakes is shown in Figure 1f, with an average dimension of 12.5 nm and a standard deviation of

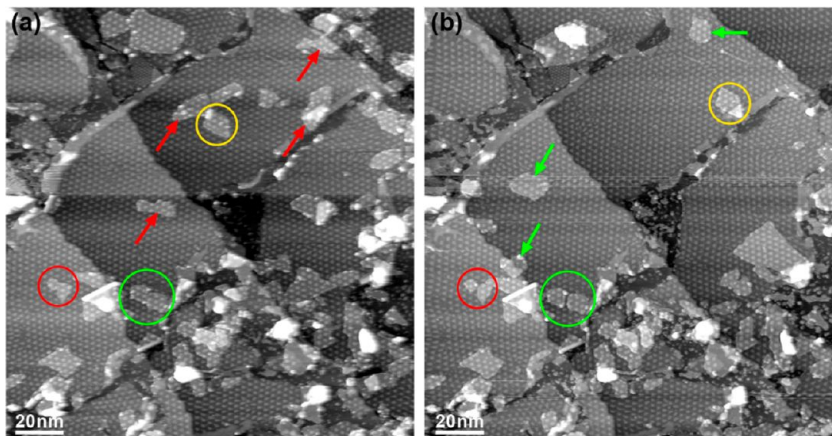


Figure 2. Successive STM images at 77 K of the same area obtained with a time interval of ~ 20 min, showing displacements of the GNFs. Some flakes moved out of the area (indicated by red arrows in (a)), while others diffused into the area (indicated by green arrows in (b)). Displacements of flakes within the area were also observed, as in the examples marked by circles. The green circles indicate two flakes that were sitting next to each other in (a) but were separated in (b) after the scanning as one of the flakes was displaced. The red circles show the same occurrence. Imaging parameters: $V_s = -2.5$ V, $I_t = 5$ pA.

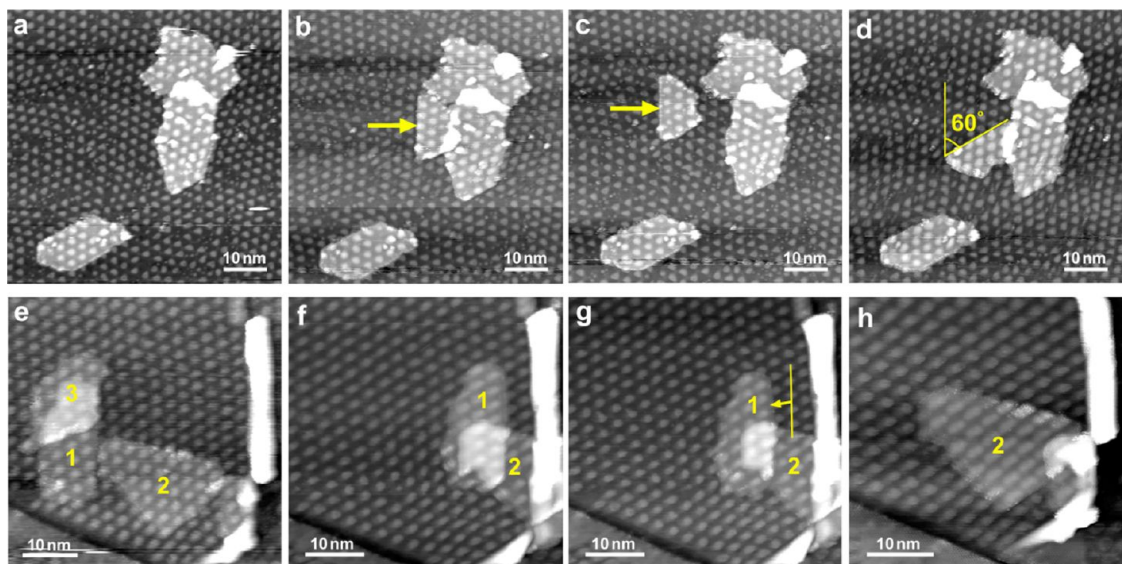


Figure 3. STM images showing the sliding behavior of GNFs on the graphene surface at 77 K. Similar displacements were also observed at 5 K. (a–d) Successive STM scans of an area with $V_s = -2.5$ V and $I_t = 5$ pA. Three flakes were initially observed in the area (a); a fourth flake moved into the area, as indicated by the arrow in (b); this flake slid to the left (c), then displaced downward and rotated by 60° (d). (e–h) Another series of images acquired with $V_s = -15$ mV and $I_t = 500$ pA. Initially three flakes, marked 1, 2, and 3, are present, with 1 and 3 partially overlapping (e). In the second image (f), flakes 1 and 2 slid to the right and overlapped, while flake 3 moved out of the area. Then flake 1 slid to the left side (g) and finally moved out of the area, with flake 2 displaced to the left (h).

2.6 nm, which is determined by the density of line defects in the as-grown graphene film.

Figure 2 shows two successive STM scans of an area with a time interval of ~ 20 min. As can be seen, the positions of the overlying GNFs have changed substantially: some flakes moved out of the area (as indicated by red arrows in Figure 2a), while others diffused into the area (as indicated by green arrows in Figure 2b). In other cases, shorter displacements within the area were observed, as pointed out by the circles in two images. For example, the green circles mark two flakes that were sitting next to each other in (a) but were separated in (b) as one of the flakes was displaced. The red circles

show the same occurrence. We found that the sliding directions of the flakes are random and are not correlated with the scanning direction.

To follow in more detail the displacements of the flakes, we acquired successive images of a specific area and tracked the movement to determine the perturbation that causes it. Figure 3 shows two series of successive scans of an area. In the first series (a–d), the images were acquired with a sample bias voltage $V_s = -2.5$ V and tunneling current $I_t = 5$ pA, corresponding to a gap resistance $R = 500$ G Ω . Three flakes were present initially in the area, two of them partially overlapping in the upper part (a); in the next image a

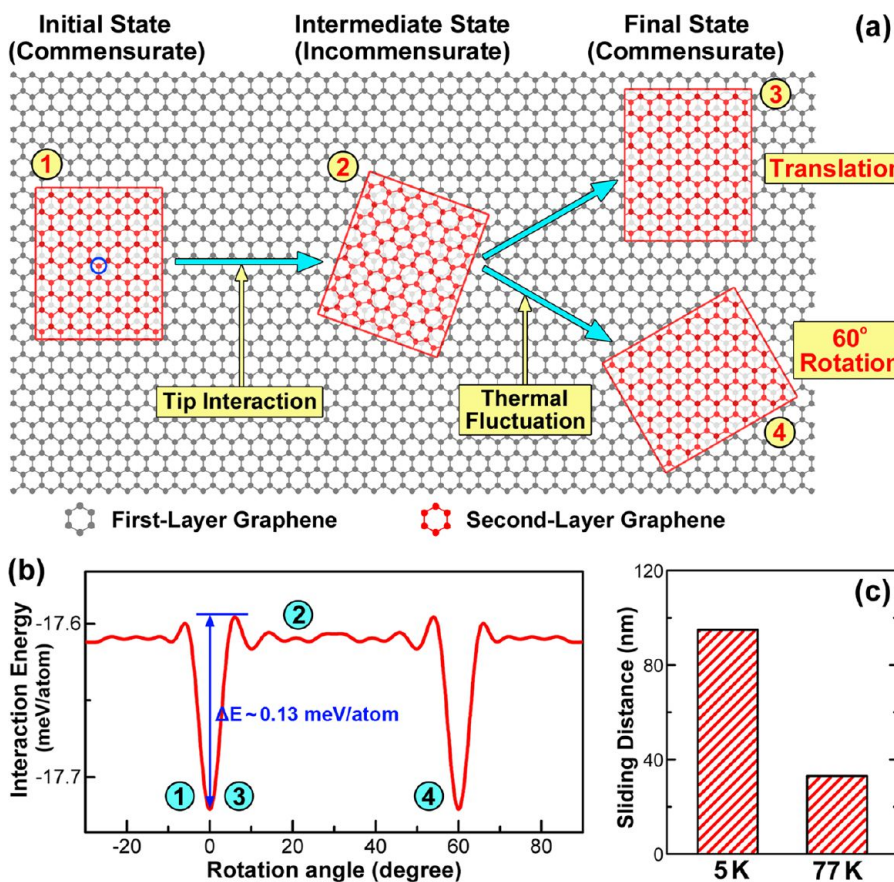


Figure 4. Proposed mechanism for the sliding of GNFs. (a) Schematic illustration showing that a flake rotates out of registry, reaching an incommensurate state (the superlubric state), where it can slide easily until another commensurate position is reached with either the same orientation or rotated by 60°. The commensurate–incommensurate transition is driven by van der Waals interactions with the STM tip, and the return to commensurate state is triggered by thermal fluctuations. (b) Plot of the interaction energy between a flake and a graphene surface as a function of the rotation angle, reproduced from ref 28 (with permission from Elsevier). The rotation axis penetrates through the atom in the top layer marked by a blue circle in (a). The four states of the flake marked in (a) are indicated respectively in the potential energy profile. (c) Average sliding distances of the flakes at 5 and 77 K.

fourth flake was found that moved into the area, as indicated by the arrow in (b); this flake slid first to the left (c) and then downward, ending up in a position rotated by 60° (d). The second series of images (e–h) were acquired with $V_s = -15 \text{ mV}$ and $I_t = 500 \text{ pA}$ ($R = 30 \text{ M}\Omega$). The first shows three flakes marked 1, 2, and 3, with flake 1 overlapping flake 3 (e). In the next image (f), flakes 1 and 2 slid to the right and end up overlapping, while flake 3 moved out of the area. Then flake 1 slid leftward by about 3 nm (g) and finally moved out of the area, while flake 2 was displaced to the left (h). In all these images the flakes always sit in commensurate positions with respect to the underlying graphene layer, either maintaining the same lattice orientation or rotating by 60°, conforming to the energetically most stable stacking.

To understand the diffusion process, we must consider the interlayer energy landscape of the graphene flakes as they move on the graphene layer. The easiest sliding path should follow the lowest corrugation in the energy landscape, and this necessarily involves incommensurate states. Several theoretical studies have been

reported on the interlayer potential landscape between graphene layers.^{16,28,34,35} While the different calculation methods give rise to different energy values, the interaction energy profiles are mostly consistent, enabling the analysis of the easiest sliding path. For example, Shibuta *et al.* used a Lennard-Jones potential to calculate energy profiles for displacements along various directions between two graphene layers²⁸ and obtained a barrier of 0.15 meV/atom for translations between commensurate states along the zigzag direction, while between incommensurate states (with rotational angle $10^\circ < \theta < 50^\circ$), the corrugation of the energy landscape is less than 0.02 meV/atom. So, it is clear that while the motion of a flake between commensurate states is hindered by numerous energy hills, it is much easier along a path connecting incommensurate states. Therefore we propose that the flakes first switch from a commensurate to an incommensurate registry with the underlying graphene layer (the superlubric state), followed by rapid sliding until another commensurate position is reached, as schematically illustrated in Figure 4a. The rate-limiting step in

the diffusion process is the initial commensurate–incommensurate transition, with a barrier of 0.13 meV/atom according to the calculations in ref 28 (Figure 4b) or 0.37 meV/atom in ref 16.

We now discuss whether the transition is activated by thermal fluctuations or by interaction with the tip. Our first experiments were performed at $T = 77$ K, corresponding to a thermal energy of $k_B T = 6.6$ meV, much lower than the transition barrier for flakes containing 4000 atoms as in our study, so thermal excitation is unlikely to activate the transition. To further confirm this, we also performed experiments at 5 K and found that the flakes show similar sliding behavior (Figure S3 in the Supporting Information). This definitely eliminates thermal agitation and leaves the tip–sample interactions as the only possible source of dragging force.³⁶ The major interactions between the tip and sample are electrostatic and van der Waals forces, which will be considered here. The electrostatic force $F_{\text{elec}} = (1/2)(\partial C/\partial z)(\Delta V)^2$, with C and ΔV being the capacitance and voltage difference between the tip and sample, is parabolic with respect to the voltage. The van der Waals force on the other hand depends only on the tip–sample distance. We performed experiments changing the imaging parameters from (−25 mV, 5 pA) to (−2.5 V, 500 pA), which maintains the same tunneling resistance ($R = 5$ GΩ) and thus a very similar tip–sample distance. Nevertheless, we found that there was no difference on the flake displacements, so the electrostatic force was excluded. Instead, we found that the flake displacements depend primarily on the tip–sample distance: the smaller the distance, the easier the displacements, such as the examples in Figure 3. Thus, we arrive at the conclusion that the van der Waals force must be at the origin of the initial motions. This interaction may result in vertical displacement of the flakes³⁶ and weakening of the interlayer binding,^{34,35} thus facilitating the transition to incommensurate states. An estimation of the van der Waals force using our experimental parameters (tip radius, tip–sample distance, and Hamaker constant) does indeed give values in the range of several 100 pN (see Figure S4 in the Supporting Information), which is of the right order of magnitude.

Once activated to the incommensurate states, the flakes can diffuse over a certain distance before they are finally locked in their equilibrium configuration.³⁷ Their random sliding directions indicate that their motions are not dominated by the STM tip anymore, but statistical fluctuations. A measurement of the stability of the superlubric state is obtained by measuring the average sliding distance of the flakes. We found that at 77 and 5 K the average displacements after sliding are about 33 and 95 nm, respectively (Figure 4c). Counterintuitively, the flakes exhibit a longer sliding distance at a lower temperature. The lifetime of the superlubric state, and thus the sliding distance, is

determined by the rate of transitions back to the commensurate ground states.³⁸ Theoretical studies by de Wijn *et al.* indicate that the stability of superlubric sliding depends on several parameters such as temperature and flake size,^{39,40} with lower temperature and larger flake size being favorable for superlubric sliding. This is consistent with our observation of longer sliding distance at lower temperature, as it is thermal fluctuations that destroy the superlubric sliding and cause them to return to ground states. However, the effect of flake size on the stability of superlubric sliding could not be verified here, as the flakes in our study have a narrow size distribution (12.5 ± 2.6 nm).

Our study is significantly different from that in ref 8, in which a graphite flake is fixed to the FFM tip and forced to slide on the surface by the tip, so the trajectory of the flake is restricted. In contrast, our study deals with free flakes sitting on a graphene surface that are only disturbed by the tip in the initial stage, following afterward a free motion along pathways of minimum energy. It is also interesting to compare our results with a previous study of the sliding and rolling of carbon nanotubes on a graphite surface using atomic force microscopy.⁴¹ Despite the similar systems (both carbon nanostructures on a graphite/graphene surface), they show distinct sliding behavior on the surface, the GNFs moving much more easily over longer distances.

Our findings provide insights for the rational design and use of graphene flakes in nanomechanical applications, such as nanolubricants,³ nanomotors,^{42–44} and movable components in NEMS devices.⁴ For example, the translational and rotational motions of GNFs can be employed for the design of nanoscale engines.⁴² It is also suggested from our study that few-layer graphene stacked with nanoscale flakes may be a more effective nanolubricant than monolayer graphene,⁶ as nanoflakes can switch more easily to incommensurate positions, in which their superlubric sliding can greatly reduce the friction and wear, thus contributing more to lubrication.

CONCLUSIONS

In summary, we have shown that the GNFs sitting on a graphene surface exhibit a surprisingly facile sliding behavior even at a low temperature of 5 K, a phenomenon that is at the heart of superlubricity inherent in incommensurate interfaces. The flakes are stable only in commensurate positions in relation with the underlying graphene layer. Once switched to an incommensurate state, the flakes diffuse over distances of more than 100 nm until another commensurate position is reached. Our direct observations of the superlubric sliding of GNFs can help the understanding of nanotribological phenomena and their applications in nanomechanical systems. Such a sliding

behavior may also be a general phenomenon for lamellar materials with a weak layer interaction, such as molybdenum disulfide (MoS_2)⁴⁵ and hexagonal

boron nitride ($h\text{-BN}$)⁴⁶ considering their similar interlayer energy landscapes⁴⁷ which are at the origin of their low-friction properties.

METHODS

The experiments were performed using a home-built, low-temperature ultrahigh-vacuum (UHV) STM operated at a base pressure below 3×10^{-11} Torr.⁴⁸ The Ru(0001) surface was cleaned first by argon ion sputtering at 1 kV, followed by annealing and cooling cycles in a partial oxygen atmosphere to remove carbon impurities from the surface. The remaining oxygen on the surface was removed by annealing the sample to 1670 K in UHV. The cleanliness of the surface was confirmed by Auger electron spectroscopy and STM. Epitaxial graphene was prepared by exposing the Ru(0001) sample to ethylene at 1230 K ($\sim 2 \times 10^{-7}$ Torr, 2 min). The sample was then slowly cooled down and transferred to the STM stage located in a connected UHV chamber. Water (Sigma Aldrich, deuterium depleted, 99.99995%) was purified by freeze–pump–thaw cycles and dosed through a leak valve and a dosing tube pointing toward the sample at a defined sample temperature. After the adsorption of submonolayer amounts of water at low temperatures (~ 110 K), the graphene film was found to be split along line defects into numerous flakes. The study presented here focuses on the movements of the resulting flakes on the surface. The STM imaging was performed using electrochemically etched Pt–Rh (70–30%) tips at either 77 or 5 K. Most STM images presented here were acquired at 77 K, unless otherwise mentioned.

Conflict of Interest: The authors declare no competing financial interest.

Acknowledgment. This work was supported by the Office of Basic Energy Sciences, Division of Materials Sciences and Engineering of the U.S. DOE, under Contract No. DE-AC02-05CH11231. S.K. and J.Y.P. acknowledge support by the WCU (World Class University) program (R-31-2008-000-10055-0) and KRF-2010-0005390 through the National Research Foundation of Korea. We thank Dr. Yasushi Shibuta for his kind permission and help on the data reproduction from ref 28.

Supporting Information Available: Figures S1–S4 showing additional STM images of the as-grown graphene film on Ru(0001); water-induced splitting of the graphene and the resulting graphene flakes; sliding behavior of the flakes on a graphene surface at 5 K; estimation of the van der Waals force between the tip and flakes. This material is available free of charge via the Internet at <http://pubs.acs.org>.

REFERENCES AND NOTES

1. Carpick, R. W.; Salmeron, M. Scratching the Surface: Fundamental Investigations of Tribology with Atomic Force Microscopy. *Chem. Rev.* **1997**, *97*, 1163–1194.
2. Mate, C. M.; McClelland, G. M.; Erlandsson, R.; Chiang, S. Atomic-Scale Friction of a Tungsten Tip on a Graphite Surface. *Phys. Rev. Lett.* **1987**, *59*, 1942–1945.
3. Kim, K. S.; Lee, H. J.; Lee, C.; Lee, S. K.; Jang, H.; Ahn, J. H.; Kim, J. H.; Lee, H. J. Chemical Vapor Deposition-Grown Graphene: The Thinnest Solid Lubricant. *ACS Nano* **2011**, *5*, 5107–5114.
4. Bunch, J. S.; van der Zande, A. M.; Verbridge, S. S.; Frank, I. W.; Tanenbaum, D. M.; Parpia, J. M.; Craighead, H. G.; McEuen, P. L. Electromechanical Resonators from Graphene Sheets. *Science* **2007**, *315*, 490–493.
5. Zheng, J.; Guo, P.; Ren, Z.; Jiang, Z.; Bai, J.; Zhang, Z. Conductance Fluctuations as a Function of Sliding Motion in Bilayer Graphene Nanoribbon Junction: A First-Principles Investigation. *Appl. Phys. Lett.* **2012**, *101*, 083101.
6. Filleter, T.; McChesney, J. L.; Bostwick, A.; Rotenberg, E.; Emtsev, K. V.; Seyller, Th.; Horn, K.; Bennewitz, R. Friction and Dissipation in Epitaxial Graphene Films. *Phys. Rev. Lett.* **2009**, *102*, 086102.
7. Lee, C.; Li, Q.; Kalb, W.; Liu, X. Z.; Berger, H.; Carpick, R. W.; Hone, J. Frictional Characteristics of Atomically Thin Sheets. *Science* **2010**, *328*, 76–80.
8. Dienwiebel, M.; Verhoeven, G. S.; Pradeep, N.; Frenken, J. W. M.; Heimberg, J. A.; Zandbergen, H. W. Superlubricity of Graphite. *Phys. Rev. Lett.* **2004**, *92*, 126101.
9. Verhoeven, G. S.; Dienwiebel, M.; Frenken, J. W. M. Model Calculations of Superlubricity of Graphite. *Phys. Rev. B* **2004**, *70*, 165418.
10. Dienwiebel, M.; Pradeep, N.; Verhoeven, G. S.; Zandbergen, H. W.; Frenken, J. W. M. Model Experiments of Superlubricity of Graphite. *Surf. Sci.* **2005**, *576*, 197–211.
11. Shinjo, K.; Hirano, M. Dynamics of Friction: Superlubric State. *Surf. Sci.* **1993**, *283*, 473–478.
12. Hirano, M.; Shinjo, K.; Kaneko, R.; Murata, Y. Observation of Superlubricity by Scanning Tunneling Microscopy. *Phys. Rev. Lett.* **1997**, *78*, 1448–1451.
13. Cumings, J.; Zettl, A. Low-Friction Nanoscale Linear Bearing Realized from Multiwall Carbon Nanotubes. *Science* **2000**, *289*, 602–604.
14. Zheng, Q. S.; Jiang, B.; Liu, S. P.; Weng, Y. X.; Lu, L.; Xue, Q. K.; Zhu, J.; Jiang, Q.; Wang, S.; Peng, L. M. Self-Retracting Motion of Graphite Microflakes. *Phys. Rev. Lett.* **2008**, *100*, 067205.
15. Liu, Z.; Yang, J. R.; Grey, F.; Liu, J. Z.; Liu, Y. L.; Wang, Y. B.; Yang, Y. L.; Cheng, Y.; Zheng, Q. S. Observation of Microscale Superlubricity in Graphite. *Phys. Rev. Lett.* **2012**, *108*, 205503.
16. Lebedeva, I. V.; Knizhnik, A. A.; Popov, A. M.; Ershova, O. V.; Lozovik, Y. E.; Potapkin, B. V. Fast Diffusion of a Graphene Flake on a Graphene Layer. *Phys. Rev. B* **2010**, *82*, 155460.
17. Popov, A. M.; Lebedeva, I. V.; Knizhnik, A. A.; Lozovik, Y. E.; Potapkin, B. V. Commensurate-Incommensurate Phase Transition in Bilayer Graphene. *Phys. Rev. B* **2011**, *84*, 045404.
18. Popov, A. M.; Lebedeva, I. V.; Knizhnik, A. A.; Lozovik, Y. E.; Potapkin, B. V. Barriers to Motion and Rotation of Graphene Layers Based on Measurements of Shear Mode Frequencies. *Chem. Phys. Lett.* **2012**, *536*, 82–86.
19. Xu, L.; Ma, T. B.; Hu, Y. Z.; Wang, H. Molecular Dynamics Simulation of the Interlayer Sliding Behavior in Few-Layer Graphene. *Carbon* **2012**, *50*, 1025–1032.
20. Feng, X.; Maier, S.; Salmeron, M. Water Splits Epitaxial Graphene and Intercalates. *J. Am. Chem. Soc.* **2012**, *134*, 5662–5668.
21. Marchini, S.; Günther, S.; Wintterlin, J. Scanning Tunneling Microscopy of Graphene on Ru(0001). *Phys. Rev. B* **2007**, *76*, 075429.
22. Martoccia, D.; Willmott, P. R.; Brugger, T.; Björck, M.; Günther, S.; Schlepütz, C. M.; Cervellino, A.; Pauli, S. A.; Patterson, B. D.; Marchini, S.; et al. Graphene on Ru(0001): A 25×25 Supercell. *Phys. Rev. Lett.* **2008**, *101*, 126102.
23. Banhart, F.; Kotakoski, J.; Krasheninnikov, A. V. Structural Defects in Graphene. *ACS Nano* **2011**, *5*, 26–41.
24. Man, K. L.; Altman, M. S. Small-Angle Lattice Rotations in Graphene on Ru(0001). *Phys. Rev. B* **2011**, *84*, 235415.
25. Altenburg, S. J.; Kröger, J.; Wang, B.; Bocquet, M. L.; Lorente, N.; Berndt, R. Graphene on Ru(0001): Contact Formation and Chemical Reactivity on the Atomic Scale. *Phys. Rev. Lett.* **2010**, *105*, 236101.
26. Zhou, M.; Lu, Y. H.; Cai, Y. Q.; Zhang, C.; Feng, Y. P. Adsorption of Gas Molecules on Transition Metal Embedded Graphene: A Search for High-Performance Graphene-Based Catalysts and Gas Sensors. *Nanotechnology* **2011**, *22*, 385502.
27. Tan, C.; Rodriguez-Lopez, J.; Parks, J. J.; Ritzert, N. L.; Ralph, D. C.; Abruna, H. D. Reactivity of Monolayer Chemical

Vapor Deposited Graphene Imperfections Studied Using Scanning Electrochemical Microscopy. *ACS Nano* **2012**, *6*, 3070–3079.

28. Shibuta, Y.; Elliott, J. A. Interaction between Two Graphene Sheets with a Turbostratic Orientational Relationship. *Chem. Phys. Lett.* **2011**, *512*, 146–150.

29. Wang, B.; Bocquet, M. L. Interfacial Coupling in Rotational Monolayer and Bilayer Graphene on Ru(0001) from First Principles. *Nanoscale* **2012**, *4*, 4687–4693.

30. Feng, X.; Salmeron, M. Electronic Screening in Stacked Graphene Flakes Revealed by Scanning Tunneling Microscopy. *Appl. Phys. Lett.* **2013**, DOI: 10.1063/1.4790382.

31. Sutter, E.; Acharya, D. P.; Sadowski, J. T.; Sutter, P. Scanning Tunneling Microscopy on Epitaxial Bilayer Graphene on Ruthenium(0001). *Appl. Phys. Lett.* **2009**, *94*, 133101.

32. Sutter, P.; Hybertsen, M. S.; Sadowski, J. T.; Sutter, E. Electronic Structure of Few-Layer Epitaxial Graphene on Ru(0001). *Nano Lett.* **2009**, *9*, 2654–2660.

33. Papagno, M.; Pacile, D.; Topwal, D.; Moras, P.; Sheverdyeva, P. M.; Natterer, F. D.; Lehnert, A.; Rusponi, S.; Dubout, Q.; Calleja, F.; et al. Two Distinct Phases of Bilayer Graphene Films on Ru(0001). *ACS Nano* **2012**, *6*, 9299–9304.

34. Kolmogorov, A. N.; Crespi, V. H. Registry-Dependent Interlayer Potential for Graphitic Systems. *Phys. Rev. B* **2005**, *71*, 235415.

35. Spanu, L.; Sorella, S.; Galli, G. Nature and Strength of Interlayer Binding in Graphite. *Phys. Rev. Lett.* **2009**, *103*, 196401.

36. Wong, H. S.; Durkan, C.; Chandrasekhar, N. Tailoring the Local Interaction between Graphene Layers in Graphite at the Atomic Scale and Above Using Scanning Tunneling Microscopy. *ACS Nano* **2009**, *3*, 3455–3462.

37. Depondt, Ph.; Ghazali, A.; Lévy, J. C. S. Self-Locking of a Modulated Single Overlay in a Nanotribology Simulation. *Surf. Sci.* **1998**, *419*, 29–37.

38. Filippov, A. E.; Dienwiebel, M.; Frenken, J. W. M.; Klafter, J.; Urbakh, M. Torque and Twist against Superlubricity. *Phys. Rev. Lett.* **2008**, *100*, 046102.

39. de Wijn, A. S.; Fusco, C.; Fasolino, A. Stability of Superlubric Sliding on Graphite. *Phys. Rev. E* **2010**, *81*, 046105.

40. de Wijn, A. S.; Fasolino, A.; Filippov, A. E.; Urbakh, M. Low Friction and Rotational Dynamics of Crystalline Flakes in Solid Lubrication. *Europhys. Lett.* **2011**, *95*, 66002.

41. Falvo, M. R.; Taylor, R. M.; Helser, A.; Chi, V.; Brooks, F. P.; Washburn, S. Superfine, R. Nanometre-Scale Rolling and Sliding of Carbon Nanotubes. *Nature* **1999**, *397*, 236–238.

42. Fleishman, D.; Klafter, J.; Porto, M.; Urbakh, M. Mesoscale Engines by Nonlinear Friction. *Nano Lett.* **2007**, *7*, 837–842.

43. Kay, E. R.; Leigh, D. A.; Zerbetto, F. Synthetic Molecular Motors and Mechanical Machines. *Angew. Chem., Int. Ed.* **2007**, *46*, 72–191.

44. Marago, O. M.; Bonaccorso, F.; Saija, R.; Privitera, G.; Guciardi, P. G.; Iati, M. A.; Calogero, G.; Jones, P. H.; Borghese, F.; Denti, P.; et al. Brownian Motion of Graphene. *ACS Nano* **2010**, *4*, 7515–7523.

45. Martin, J. M.; Donnet, C.; Le Mogne, Th.; Epicier, Th. Superlubricity of Molybdenum Disulphide. *Phys. Rev. B* **1993**, *48*, 10583–10586.

46. Marom, N.; Bernstein, J.; Garel, J.; Tkatchenko, A.; Joselevich, E.; Kronik, L.; Hod, O. Stacking and Registry Effects in Layered Materials: The Case of Hexagonal Boron Nitride. *Phys. Rev. Lett.* **2010**, *105*, 046801.

47. Hod, O. Interlayer Commensurability and Superlubricity in Rigid Layered Materials. *Phys. Rev. B* **2012**, *86*, 075444.

48. Shimizu, T. K.; Mugarza, A.; Cerda, J. I.; Heyde, M.; Qi, Y. B.; Schwarz, U. D.; Ogletree, D. F.; Salmeron, M. Surface Species Formed by the Adsorption and Dissociation of Water Molecules on a Ru(0001) Surface Containing a Small Coverage of Carbon Atoms Studied by Scanning Tunneling Microscopy. *J. Phys. Chem. C* **2008**, *112*, 7445–7454.